THE JOURNAL OF PHYSICAL CHEMISTRY LETTERS
A JOURNAL OF THE AMERICAN CHEMICAL SOCIETY

pubs.acs.org/JPCL

Letter

Photoreactive Carbon Dioxide Capture by a Zirconium–Nanographene Metal–Organic Framework

Xin Zheng, Matthew C. Drummer, Haiying He, Thomas M. Rayder, Jens Niklas, Nicholas P. Weingartz, Igor L. Bolotin, Varun Singh, Boris V. Kramar, Lin X. Chen, Joseph T. Hupp, Oleg G. Poluektov, Omar K. Farha, Peter Zapol, and Ksenija D. Glusac*

Cite This: *J. Phys. Chem. Lett.* 2023, 14, 4334–4341

Read Online

ACCESS | Metrics & More | Article Recommendations | Supporting Information

ABSTRACT: The mechanism of photochemical CO_2 reduction to formate by PCN-136, a Zr-based metal–organic framework (MOF) that incorporates light-harvesting nanographene ligands, has been investigated using steady-state and time-resolved spectroscopy and density functional theory (DFT) calculations. The catalysis was found to proceed via a "photoreactive capture" mechanism, where Zr-based nodes serve to capture CO_2 in the form of Zr–bicarbonates, while the nanographene ligands have a dual role of absorbing light and storing one-electron equivalents for catalysis. We also find that the process occurs via a "two-for-one" route, where a single photon initiates a cascade of electron/hydrogen atom transfers from the sacrificial donor to the CO_2-bound MOF. The mechanistic findings obtained here illustrate several advantages of MOF-based architectures in molecular photocatalyst engineering and provide insights on ways to achieve high formate selectivity.

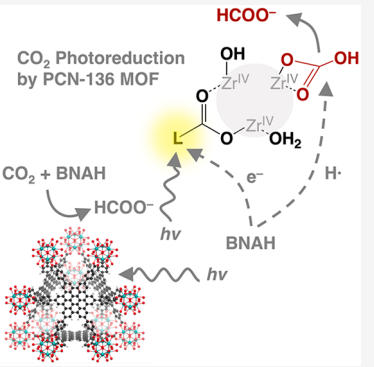

Metal–organic frameworks (MOFs) are excellent scaffolds for the design of heterogeneous photocatalysts because they enable self-assembly of light-harvesting chromophores and catalysts into ordered arrays of porous crystals for efficient substrate adsorption and subsequent conversion.[1−8] While initial studies proposed a semiconductor model of photoactive MOFs to explain their broad UV–vis absorption edges falling within semiconductor band gaps,[9,10] this model has since been discounted based on weak coupling between distant chromophores, attribution of broad absorption to inhomogeneous broadening, poor overlap between frontier orbitals, lack of band dispersion in the electronic structure, and low charge mobility leading to low photoconductance.[11−13] Despite the growing consensus that MOFs behave like an ordered array of self-assembled molecular catalysts,[12,14] the strengths of MOFs as highly porous heterogeneous catalysts and the spatial confinement of molecular components in MOF assemblies[15] leading to electronic properties greater than "sum of their parts" should not be undervalued.[14] Among the materials with the highest porosity, MOFs have a high density of active surface sites available for catalysis, facile diffusion of reactants, and separation of products.[3,5] Different aspects of MOF architecture including pore sizes and shapes, morphology, etc., are highly tunable with nearly infinite selection of organic or organometallic linkers and metal nodes, while postsynthetic modifications can be utilized to incorporate additional catalytic species or spectators that may orient reactants favorably or stabilize transition state structures.[7] Furthermore, the proximity and confinement of different components of a photocatalytic system—light harvester, photosensitizer, catalyst, sacrificial agent and substrate—shorten mass transfer and charge migration distances, thus improving the overall efficiency.[1−3,16]

Beginning with the first study using NH2-MIL-125(Ti) for photoreduction of carbon dioxide to the formate anion $HCOO^-$ in 2012,[17] MOFs and their derivatives have been actively explored in the past decade as a new class of carbon dioxide reduction photocatalysts.[1−8] This work is motivated by the need to mitigate the effects of carbon dioxide on climate change by its conversion into carbon-neutral fuels and value-added chemicals (carbon monoxide, formic acid, methane, methanol, etc.) using sustainable energy resources, such as sunlight. MOFs enable selective adsorption and high uptake of CO_2 using functionalized or hydrophobic linkers, providing a high local concentration of CO_2 around the catalytic site, while the competing hydrogen evolution reaction can be suppressed.[3] Zirconium-based MOFs are often utilized in photocatalytic CO_2 reductions, because Zr-carboxylate MOFs are formed via strong coordination bonds between the Zr^{4+} ions of the secondary building units (hard acid) and the

Received: January 8, 2023
Accepted: April 5, 2023
Published: May 3, 2023

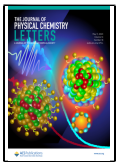

Downloaded via UNIV OF ILLINOIS CHICAGO on June 2, 2023 at 15:17:01 (UTC).
See https://pubs.acs.org/sharingguidelines for options on how to legitimately share published articles.

ACS Publications
© 2023 American Chemical Society

carboxylate O of the ligands (hard base).[18] The stability of Zr-MOFs in organic solvents and aqueous acidic conditions[18,19] combined with the abundance of Zr in nature and low toxicity of Zr in biological systems have led to growing numbers of Zr-MOFs reported in recent literature.[18] Many Zr-MOFs with amine-functionalized linkers,[20−24] highly conjugated linkers,[21−26] metalloligands,[27,28] mixed ligands,[24,29] node- or ligand-grafted molecular catalysts or single-atom catalysts,[29−36] and enzyme encapsulation[37] have been shown to catalytically convert CO_2 to $HCOO^-$, CO, CH_4, CH_3OH, and CH_3CH_2OH under visible light irradiation in the presence of sacrificial electron donors or water.

Even in the absence of any additional catalytic units, Zr-based MOFs have been shown to photocatalytically convert CO_2 selectively to $HCOO^-$. While the catalytic performance has been reported in many studies,[20−26,38] the catalytic site responsible for conversion and mechanistic details remain unclear. This is in contrast to Ti-based MOFs with small organic ligands, such as NH_2-MIL-125(Ti), for which an evident photochromic effect, unambiguous electron paramagnetic resonance (EPR) spectroscopy data, and transient absorption (TA) photolysis experiments confirm that the photoinduced generation of Ti(III) ions occurs from ligand to metal charge transfer (LMCT) excited states and that these reduced node metal centers are responsible for catalytic conversion of CO_2 to $HCOO^-$.[2,39] Whether LMCT states cause reduction of Zr(IV) to Zr(III) in the Zr_6-oxo clusters is currently open to debate. Many studies on Zr-MOFs for photocatalytic CO_2 reduction have provided EPR, UV−vis diffuse reflectance, photoluminescence, and ultrafast transient absorption data showing evidence of charge transfer from excited state ligand to Zr-oxo cluster, reduction of Zr^{4+} to Zr^{3+}, and subsequent CO_2 to formate reduction by Zr^{3+}.[20−26,38] In contrast, other studies controvert the possibility of node reduction, based on the lack of EPR signal ascribable to Zr(III) and lack of photocatalytic activity in Zr-MOFs.[40,41] Computational studies indicate that the empty d-orbitals of Zr do not overlap with the ligand π^* orbitals and that electronic transitions in Zr-MOFs are purely ligand-based and cannot result in formation of Zr(III) via LMCT.[40,42,43] Finally, a recent study showed a non-innocent role of the sacrificial electron donor TEOA and argues that the photoreduction of CO_2 begins with the photooxidation of TEOA to generate TEOA* radicals that serve as hydride donors to reduce thermally activated CO_2 at the Zr_6 Lewis acid nodes.[44,45]

Given the contrasting conclusions drawn from previous studies regarding the photochemical mechanism of formate formation, we report here a mechanistic study of photochemical reduction of CO_2 by **PCN-136**, a Zr-based MOF that contains nanographene-based, hexakis(4-carboxyphenyl)-hexabenzocoronene, $\mathbf{HCHC^{6-}}$ ligands (Scheme 1). The synthesis of **PCN-136** was reported previously by the Zhou team, who elegantly circumvented the challenges associated with the low solubility of $\mathbf{HCHC\text{-}H_6}$ by performing a postsynthetic nanographene planarization.[26] The authors showed that **PCN-136** absorbs light throughout the entire UV/vis range and that it photocatalytically reduces CO_2 selectively to formate. Here, we build on this work by exploring the mechanism of CO_2 reduction using steady-state and time-resolved photochemistry experiments coupled with density functional theory (DFT) calculations. Our work provides strong evidence that the photochemical reduction of CO_2 occurs via a "photoreactive capture" mechanism in which

Scheme 1. Photochemical CO_2 Reduction to Formate by a Zr-Nanographene MOF PCN-136[a]

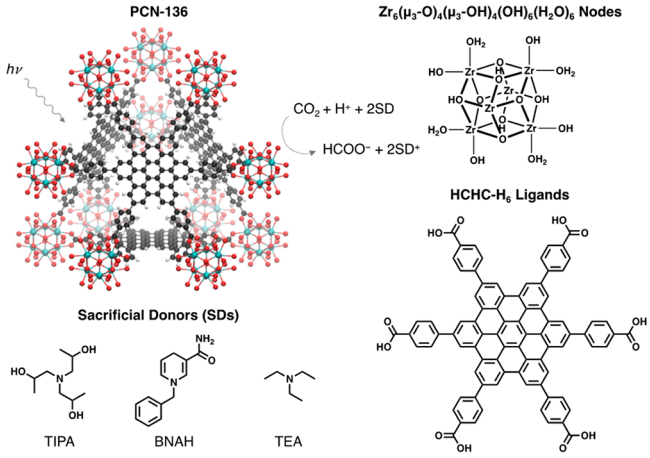

[a]**PCN-136** ball-and-stick structure: black for carbon, blue for zirconium, red for oxygen, white for hydrogen; the MOF is made of $Zr_6(\mu_3\text{-}O)_4(\mu_3\text{−}OH)_4(OH)_6(H_2O)_6$ nodes and $\mathbf{HCHC\text{-}H_6}$ conjugate acid form of the ligand (hydroxide and aqua ligands of two of the Zr's in the node are omitted for clarity); sacrificial electron donors used for the study of photochemical reduction are triisopropanolamine (TIPA), 1-benzyl-1,4-dihydronicotinamide (BNAH) and triethylamine (TEA).

CO_2 is first captured by the MOF node in the form of a Zr−bicarbonate adduct. It is then photochemically reduced via photoinduced electron transfer from nanographene-based ligand-centered excited states of the MOF. The results of this work opened the possibility of using MOF building blocks not just for gas capture/release schemes, but also for combined capture and direct conversion to value-added chemicals.

To obtain insights into the possible reaction mechanism, computational investigation using DFT was performed (Section S1). The calculated density of states of **PCN-136**, indicates that the frontier orbitals are mostly located on the C atoms of the ligand (Figure S1) and also explains the previously reported narrowing of the experimental bandgap to 1.18 eV upon postsynthetic ligand modification.[26] Based on these results, we conclude that the light absorption by **PCN-136** will lead to π−π^* transitions and that the photoreduction by a sacrificial donor (SD) will generate ligand-centered radical ions as opposed to reduced Zr-centers on the MOF node. This conclusion is further supported by the calculated energy landscape for the CO_2 reduction to formate involving Zr-reduction ("catalytic node" mechanism, Figure S2), which shows that the reduction of Zr(IV) center to the corresponding Zr(III) ion in the node requires 2.77 eV. Given that the calculated bandgap of **PCN-136** is much smaller, we conclude that the photochemical reduction of the Zr(IV) ion is not likely to occur. We also explored the possibility of CO_2-to-formate conversion catalyzed by the ligand and found that this reaction pathway requires 1.77 eV of energy, which is again more than the bandgap ("catalytic ligand" mechanism, Figure S3). This calculation is consistent with the experimental finding that ligand alone cannot reduce CO_2 to formate with triisopropanolamine (TIPA) as SD.[26]

Interestingly, our calculations indicate that the "photoreactive capture" mechanism shown in Figure 1, which occurs via the insertion of CO_2 into the Zr−OH bond of the node, provides a low-energy reaction pathway for CO_2-to-formate

https://doi.org/10.1021/acs.jpclett.3c00049
J. Phys. Chem. Lett. 2023, 14, 4334−4341

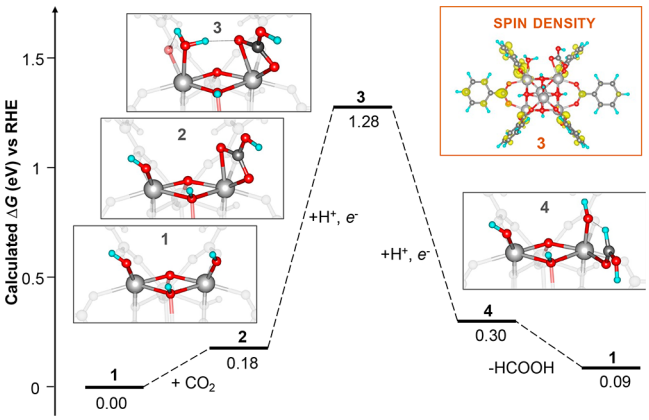

Figure 1. Calculated Gibbs free energies for photoreactive CO_2 capture mechanism. The Gibbs free energy is shown below the line, and the numbering of structures is shown above the line at each step; the spin density distribution for **3** is shown in the upper-right corner. (Color code for computed structures: Zr, light gray; O, red; H, blue; C, dark gray; spin densities, yellow.)

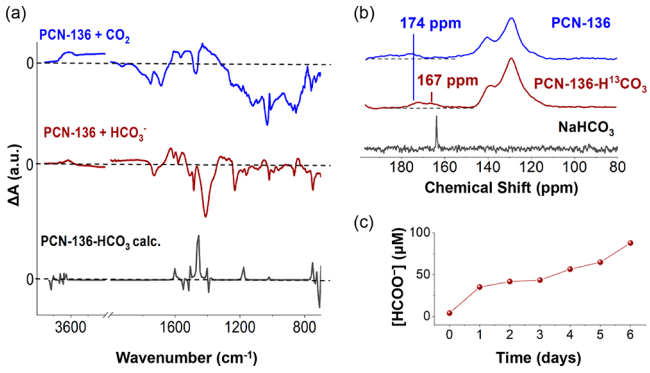

Figure 2. Experimental support for the "photoreactive capture" mechanism: (a) IR difference absorption spectra ($\Delta A = A$[sample] − A[**PCN-136**]) of **PCN-136** purged with CO_2 (blue) or exposed to aqueous $NaHCO_3$ (red). The black spectrum shows the calculated difference IR absorption spectrum ($\Delta A = A$[**2**] − A[**1**]). (b) Solid-state CPMAS ^{13}C NMR of **PCN-136** before (blue) and after (red) $NaH^{13}CO_3$ treatment. The spectrum of $NaHCO_3$ (black) is shown for reference. (c) Formate yield as a function of irradiation time for $NaHCO_3$-treated **PCN-136** in Ar-sparged 8:1:1 acetonitrile/water/TIPA solution.

conversion. Several different CO_2 chemisorption modes were considered and the calculated Gibbs free energies were found to vary from +0.18 eV to +0.82 eV (Figure S4). The "bidentate bicarbonate Zr−O_2−COH" structure **2** (Figure 1) formed by CO_2 insertion into the Zr−OH bond was found to have the lowest ΔG value. Similar capture reactivity by insertion into the metal-hydroxide bond has been observed in natural CO_2 fixation by carbonic anhydrase[46] and has been employed for CO_2 capture.[47] Our calculations indicate that the Zr−bicarbonate adduct **2**, once formed, can be efficiently reduced to the formate ion with relatively low energy input (Figure 1). The reduction of the bound bicarbonate **2** to form intermediate **3** requires only 1.10 eV, which is smaller than the bandgap of **PCN-136**. The reduction takes place on the ligand moiety, as confirmed by the calculated spin density distribution for adduct **3** (Figure 1), indicating that the nanographene ligand serves as the site for storage of one-electron equivalents. The second reduction step from **3** to **4** is downhill in energy, leading to the generation of formic acid. Overall, the computational results shown in Figure 1 propose a mechanism that combines CO_2 capture with its photochemical reduction to formate, which can proceed using photons with energy across the solar spectrum.

To provide experimental support for the mechanism, we synthesized **PCN-136** using a previously published procedure[48] (product characterization is provided in Section S2, Supporting Information). The formate ion was detected during photochemical reduction of CO_2 by **PCN-136** using TIPA as SD (Section S3, Supporting Information), consistent with previously published results.[26] The role of the Zr−bicarbonate adduct **2** was evaluated experimentally by investigating the conversion of **PCN-136** into the bicarbonate adduct **PCN-136-HCO_3** using two approaches (Figure 2): (i) a direct reaction between CO_2 and **PCN-136** and (ii) the reaction between aqueous bicarbonate ions and **PCN-136** (see Section S1 for more information). Pathway i was evaluated by monitoring the changes in the infrared (IR) spectra of **PCN-136** after exposure to CO_2 and after subsequent purge with argon (Figure 2a, blue trace). The exposure to CO_2 gives rise to a growth of weak absorption bands associated with OH stretching (3530−3750 cm^{-1}), CO asymmetric stretching (1500−1650 cm^{-1}), CO symmetric stretching (1420−1480 cm^{-1}), OH bending (1280−1300 cm^{-1}), COH bending (1170−1190 cm^{-1}), and COH stretching (990−1020 cm^{-1}), which can be attributed to the Zr−bicarbonate group based on the literature.[49−54] A similar difference IR spectrum was obtained when **PCN-136** was treated with $NaHCO_3$ (Figure 2a, red trace) and matches qualitatively the difference IR spectrum obtained from DFT calculated structures **2** and **1** (Figure 2a, black trace). However, the bands ascribable to bicarbonate in the IR spectra in Figures 2a, S13, and S14 are weak in intensity (similar to previously reported IR spectra[55]), precluding a more definitive assignment. The **PCN-136-HCO_3** structure formed by a treatment with $NaHCO_3$ remains crystalline (XRD, Figure S12), while the formation of the bicarbonate was further confirmed using nuclear magnetic resonance, NMR (Figure 2b). Solid-state ^{13}C NMR (Figure 2b) shows a new broad peak at 167 ppm in **PCN-136-$H^{13}CO_3$**, which can be assigned to the C atom of the Zr-bound bicarbonate group and is comparable to the literature reported ^{13}C NMR chemical shifts of Zr-carbonate/bicarbonate.[56,57] The same peak at 167 ppm is also observed for pbz-MOF-1 (the precursor MOF for **PCN-136** with the same Zr-node) after $NaH^{13}CO_3$ treatment (Figure S15).

Given that the experimental photochemical CO_2 reduction is performed in a basic solution (8:1:1 acetonitrile/water/TIPA with pH 7.2−8.2, Section S3) where bicarbonate ions are expected to dominate, we hypothesize that pathway ii is more relevant for the observed photocatalysis. It is interesting to point out that **PCN-136-HCO_3** is not likely to be formed by the Zr−OH + HCO_3^- → Zr−O_3CH (or **2**) + OH^- exchange because the driving force for this reaction is calculated to be ΔG = +1.24 eV. Instead, we hypothesize that the **PCN-136-HCO_3** formation involves exchange with the ligand, as shown in Scheme 2. This ligand/bicarbonate exchange is also supported by a previous report showing that full MOF digestion takes place when concentrated bicarbonate solutions are used[58] and the observation that our more dilute bicarbonate solutions take on a dark red color, attributable to free ligand, when they were added to **PCN-136**. We further

https://doi.org/10.1021/acs.jpclett.3c00049
J. Phys. Chem. Lett. 2023, 14, 4334−4341

Scheme 2. Proposed Mechanism of Photochemical CO_2 Reduction by PCN-136[a]

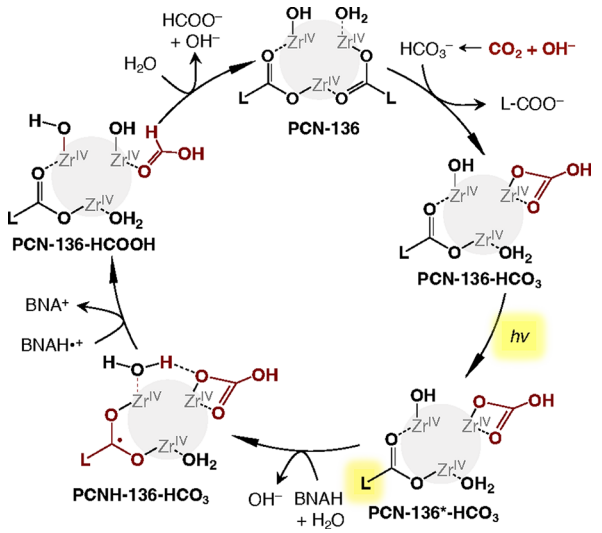

[a]The Zr-node of the MOF is represented by a shaded grey circle and three relevant Zr-centers, while L-COOH represents the **HCHC-H$_6$** ligand.

performed the photochemical reduction of **PCN-136-HCO$_3$** in the absence of CO_2 and found that the formate ions are still formed (Figure 2c). The observation of formate formation by a direct reduction of bicarbonate adduct is a strong confirmation that the "photoreactive capture" mechanism takes place.

Our investigation of the effect of SD on the product yields provided additional insights into the mechanism of the second electron transfer step (Table 1). Three SDs were studied

Table 1. Effect of SD on the Formate Yield[a]

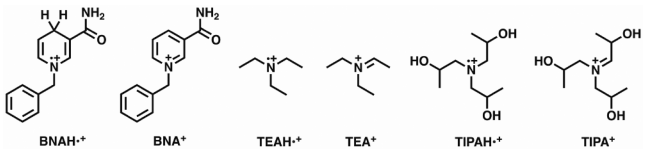

Reaction	$\Delta G_{3\rightarrow4}$ (eV)	[HCOO⁻] at 72 h (mM)	TON
BNAH$^{\bullet+}$ + **3** → **4** + BNA$^+$	−1.89	4.14	8.8
TEAH$^{\bullet+}$ + **3** → **4** + TEA$^+$	−1.61	1.17	2.5
TIPAH$^{\bullet+}$ + **3** → **4** + TIPA$^+$	−1.18	1.11	2.4

[a]The experimental formate concentration obtained after 72 h of irradiation of PCN-136 in the presence of CO_2 and different SDs. Calculated ΔG values for H-atom transfer from SD radical cations (structures shown) transfer to intermediate **3**.

(BNAH, TEA, and TIPA; structures are shown in Scheme 1), and formate was generated in all three cases. However, the formate yield increases in the TIPA < TEA < BNAH sequence (Table 1, Figure S17). Interestingly, this trend correlates with the calculated Gibbs free energies for the H atom transfer from SD radical cations to the intermediate **3** (shown in Figure 1) to form intermediate **4** (Table 1). This correlation indicates that the second reduction step may occur thermally via hydrogen-atom transfer from oxidized SD.

Time-resolved optical and EPR spectroscopy were utilized to identify early intermediates formed upon the photo-excitation of **PCN-136** (Figure 3, see Section S4 for experimental details). Femtosecond (fs) and nanosecond (ns) TA spectra and kinetic traces (Figures 3, parts a and b) indicate the presence of four different transients with broad negative signal throughout most of the visible range and a positive signal at ∼700 nm. Target analysis of TA data (Figure 3c) using a sequential 1 → 2 → 3 → 4 model provided spectral features of individual components and accompanying τ_1 = 8.1 ps, τ_2 = 140 ps, τ_3 = 1 μs, and τ_4 = 14 μs lifetimes. Time-resolved continuous wave (cw) EPR spectroscopy (Figure 3d) revealed the presence of a spin-polarized organic triplet signal. This type of polarization pattern is typical for triplet states created from optically excited singlet state by intersystem crossing (ISC) mechanism.[59−61] The line shape and zero-field splitting parameter, $D \approx 82$ mT, are similar to the triplet state EPR spectra reported previously for organic aromatic systems[62,63] In addition to the signals associated with the organic triplet state, a much narrower EPR signal with a linewidth of 1.1 mT was observed at $g \approx 2.003-2.004$ (enlarged in Figure 3d inset). This signal does not demonstrate any resolved hyperfine structure, which is indicative of an organic radical with highly delocalized electron spin density and no heavier atoms like oxygen or metals involved. This is a transient radical which decays in several microseconds after the laser flash. Consistent with the absence of stable, light-generated paramagnetic Zr species in EPR, high-resolution Zr XPS (Figures S18 and S19) also show that there is no change in oxidation state of Zr. Based on this experimental evidence, we hypothesize that the long-lived components are associated with the formation of ligand-centered T_1 triplet excited state (component **3**, which formed with an ISC time of ∼140 ps) and ligand-centered radical ions (component **4**), likely formed via symmetry breaking charge transfer mechanism from the T_1 state.[64] Since EPR evidence suggests that the T_1 state is formed directly from the singlet state, component **2** is assigned to the ligand-centered S_1 state. Component **1** is assigned to vibrationally "hot" S_1 excited state which undergoes vibrational relaxation to the S_1 state with an 8.1 ps lifetime.[65] Based on this assignment, we hypothesize that the photochemical CO_2 reduction is initiated by ligand-centered excited-states, as illustrated in Scheme 2.

Based on the experimental and computational studies described above, the mechanism for photochemical CO_2 reduction by **PCN-136** is proposed, as illustrated in Scheme 2. The catalytic cycle is initiated by the CO_2 capture step, which involves the formation of bicarbonate adduct **PCN-136-HCO$_3$** by the ligand/bicarbonate exchange from **PCN-136**. Light absorption generates the ligand-centered excited state of **PCN-136*-HCO$_3$**, as confirmed by time-resolved optical and EPR results shown in Figure 3. Subsequent reduction by a sacrificial donor BNAH via proton-coupled electron transfer leads to the intermediate **PCNH-136-HCO$_3$**, in which one of the electrons needed for CO_2/formate conversion is temporarily stored at the ligand moiety. Then, thermal H atom transfer occurs from BNAH$^{\bullet+}$ to generate the formic-acid adduct **PCN-136-HCOOH**, followed by the formate elimination and the closure of the catalytic cycle.

Several aspects of the mechanism proposed in Scheme 2 illustrate advantages of MOF-based architectures in the molecular photocatalyst engineering. First, porous 3D scaffolds of **PCN-136** bring different functional moieties into proximity, namely the light-harvesting nanographene ligands and Zr-based groups for CO_2 capture. The rigid nature of **PCN-136** prevents the undesired dimerization of ligand-based radical

https://doi.org/10.1021/acs.jpclett.3c00049
J. Phys. Chem. Lett. 2023, 14, 4334−4341

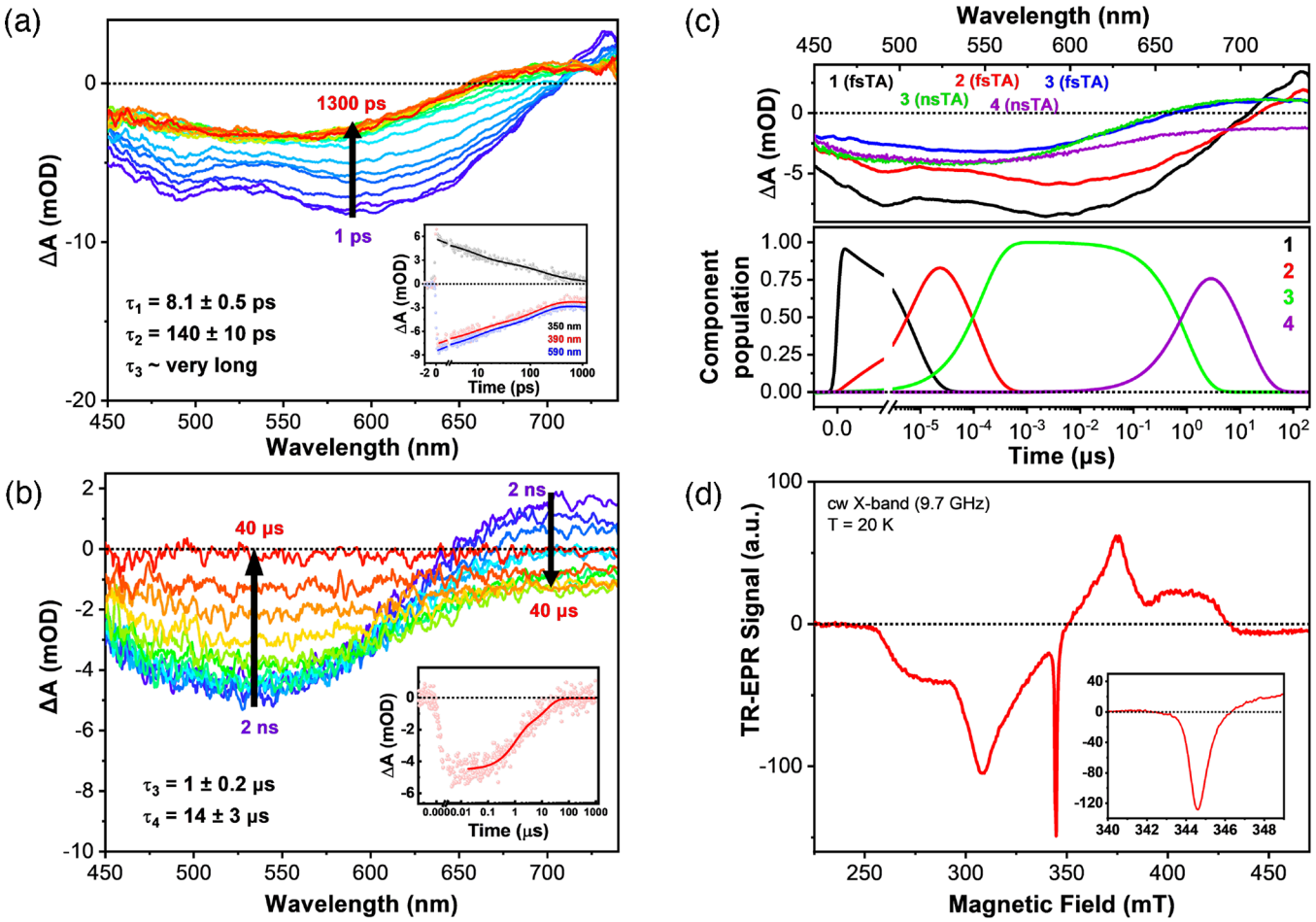

Figure 3. (a) Femtosecond and (b) nanosecond transient absorption spectra of **PCN-136** suspended in DMF probed at different delay times after 410 nm excitation; insets show kinetic traces at 350, 390, and 590 nm (panel a) and 530 nm (panel b). Solid lines in the inset show the fits using a sequential kinetic model and lifetimes listed in each panel. (c) Component spectra (top) and population kinetics (bottom) obtained using the target analysis of fsTA and nsTA data and a sequential **1** → **2** → **3** kinetic model for the fsTA data and a **3** → **4** model for the nsTA data. Both blue and green spectra are for the same component observed as the last component in the fsTA data (blue) and the first component in the nsTA data (green). (d) Photoinduced time-resolved EPR signal of **PCN-136** suspended in methanol.

cations, a process that often occurs when similar open-shell species are freely diffusing in solution.[66,67] Such improved stability of ligand-based radicals further enables utilization of ligand moieties for accumulation of "hydrogen atom equivalents" near the reactive Zr-node, as illustrated in intermediate **PCN-136-HCO$_3$**. These stored equivalents are then elegantly delivered to the reactive Zr-site via a network of coordination and hydrogen bonds across two Zr-centers during the conversion from **PCN-136-HCO$_3$** to **PCN-136-HCOOH**. Such H atom relays have been observed in other H-bonded[68] or coordination[69] compounds and play an important role in proton-coupled redox processes.

Second, the proposed mechanism combines CO_2 capture with its direct conversion to value-added products, in a process we name "photoreactive capture". Similar reactive capture schemes have recently been demonstrated as promising mechanisms for electrochemical, photochemical, and thermal carbon upgrading, because they avoid energy losses associated with the CO_2 release from capturing agents.[70−72] To enable reactive capture, the Gibbs free energies for CO_2 binding need to be finely tuned to be sufficiently exergonic for efficient gas capture and not too exergonic so that efficient conversion to value-added chemicals can take place. The work reported here illustrates that capture of CO_2 in the form of metal bicarbonates is an effective tool for reactive capture.

Finally, the CO_2/formate conversion shown in Scheme 2 involve a "two-for-one" approach, where a single photon triggers a cascade of electron/hydrogen atom transfers. Similar two-electron sensitization processes have been reported previously, and they include the reverse reaction: the conversion of formate to CO_2.[73−75] The "two-for-one" CO_2-to-formate reduction demonstrated here is likely responsible for high formate selectivity observed here and in many other photochemical CO_2 conversion experiments involving light-responsive Zr-based MOFs.[20−26,38] We anticipate that the "two-for-one" mechanism will be a valuable tool for future CO_2 reduction catalysts with improved formate selectivity.

■ ASSOCIATED CONTENT

Supporting Information

The Supporting Information is available free of charge at https://pubs.acs.org/doi/10.1021/acs.jpclett.3c00049.

Synthesis and characterization of MOFs and photochemical and computational details (PDF)

Transparent Peer Review report available (PDF)

https://doi.org/10.1021/acs.jpclett.3c00049
J. Phys. Chem. Lett. 2023, 14, 4334−4341

AUTHOR INFORMATION

Corresponding Author

Ksenija D. Glusac − *Department of Chemistry, University of Illinois at Chicago, Chicago, Illinois 60607, United States; Chemical Sciences and Engineering Division, Argonne National Laboratory, Lemont, Illinois 60439, United States;* orcid.org/0000-0002-2734-057X; Email: glusac@uic.edu

Authors

Xin Zheng − *Department of Chemistry, University of Illinois at Chicago, Chicago, Illinois 60607, United States;* orcid.org/0000-0002-5506-8112

Matthew C. Drummer − *Department of Chemistry, University of Illinois at Chicago, Chicago, Illinois 60607, United States; Chemical Sciences and Engineering Division, Argonne National Laboratory, Lemont, Illinois 60439, United States*

Haiying He − *Department of Physics and Astronomy, Valparaiso University, Valparaiso, Indiana 46383, United States;* orcid.org/0000-0002-3493-2784

Thomas M. Rayder − *Department of Chemistry, Northwestern University, Evanston, Illinois 60208, United States;* orcid.org/0000-0002-2488-1143

Jens Niklas − *Chemical Sciences and Engineering Division, Argonne National Laboratory, Lemont, Illinois 60439, United States;* orcid.org/0000-0002-6462-2680

Nicholas P. Weingartz − *Department of Chemistry, Northwestern University, Evanston, Illinois 60208, United States*

Igor L. Bolotin − *Department of Chemistry, University of Illinois at Chicago, Chicago, Illinois 60607, United States*

Varun Singh − *Department of Chemistry, University of Illinois at Chicago, Chicago, Illinois 60607, United States; Chemical Sciences and Engineering Division, Argonne National Laboratory, Lemont, Illinois 60439, United States*

Boris V. Kramar − *Department of Chemistry, Northwestern University, Evanston, Illinois 60208, United States*

Lin X. Chen − *Department of Chemistry, Northwestern University, Evanston, Illinois 60208, United States; Chemical Sciences and Engineering Division, Argonne National Laboratory, Lemont, Illinois 60439, United States;* orcid.org/0000-0002-8450-6687

Joseph T. Hupp − *Department of Chemistry, Northwestern University, Evanston, Illinois 60208, United States;* orcid.org/0000-0003-3982-9812

Oleg G. Poluektov − *Chemical Sciences and Engineering Division, Argonne National Laboratory, Lemont, Illinois 60439, United States;* orcid.org/0000-0003-3067-9272

Omar K. Farha − *Department of Chemistry, Northwestern University, Evanston, Illinois 60208, United States*

Peter Zapol − *Materials Science Division, Argonne National Laboratory, Lemont, Illinois 60439, United States;* orcid.org/0000-0003-0570-9169

Complete contact information is available at: https://pubs.acs.org/10.1021/acs.jpclett.3c00049

Notes

The authors declare the following competing financial interest(s): O.K.F. and J.T.H. acknowledge equity interests in NuMat Technologies, a company that commercializes MOFs.

ACKNOWLEDGMENTS

This work is supported by the U.S. Department of Energy (DOE), Office of Science, Office of Basic Energy Science, Division of Chemical Sciences, Geosciences, and Biosciences, through Argonne National Laboratory under Contract No. DE-AC02-06CH11357. We acknowledge the computational resources provided by the Laboratory Computing Resource Center at Argonne National Laboratory and the Center for Nanoscale Materials, a U.S. Department of Energy Office of Science User Facility, supported by the U.S. DOE, Office of Basic Energy Sciences, under Contract No. DE-AC02-06CH11357. The EPR work (O.G.P,. J.N.) was supported by the U.S. Department of Energy (DOE), Office of Basic Energy Sciences, Division of Chemical Sciences, Geosciences, and Biosciences, under Contract no. DE-AC-02-06CH11357. J.T.H. gratefully acknowledges support from the U.S. DOE, Office of Science, Basic Energy Sciences (Grant DE-FG02-87ER13808). O.K.F. and T.M.R. acknowledge a grant from Department of Energy (DE-SC0022332). We thank Rosmi Reji for her help with time-resolved spectroscopy experiments. We also thank Dr. Zhijie Chen, Dr. Subhadip Goswami, and Dr. Yang Song for suggestions regarding the pbz-MOF-1 synthesis and XRD characterization. We thank Shirin Saffar Avval and Prof. Brian Chaplin for their help with protocols for formate detection. SEM work made use of the EPIC facility of Northwestern University's NUANCE Center, which has received support from the SHyNE Resource (NSF ECCS-2025633), the IIN, and Northwestern's MRSEC program (NSF DMR-1720139).

REFERENCES

(1) Ding, M.; Flaig, R. W.; Jiang, H. L.; Yaghi, O. M. Carbon Capture and Conversion Using Metal-Organic Frameworks and MOF-Based Materials. *Chem. Soc. Rev.* **2019**, *48* (10), 2783−2828.

(2) Li, R.; Zhang, W.; Zhou, K. Metal-Organic-Framework-Based Catalysts for Photoreduction of CO2. *Adv. Mater.* **2018**, *30* (35), No. 1705512.

(3) Zhan, W. W.; Gao, H.; Yang, Y.; Li, X. F.; Zhu, Q. L. Rational Design of Metal-Organic Framework-Based Materials for Photocatalytic CO2 Reduction. *Adv. Energy Sust. Res.* **2022**, *3* (7), 2200004.

(4) Guo, K.; Hussain, I.; Jie, G. A.; Fu, Y. H.; Zhang, F. M.; Zhu, W. D. Strategies for Improving the Photocatalytic Performance of Metal-Organic Frameworks for CO2 Reduction: A Review. *J. Environ. Sci.* **2023**, *125*, 290−308.

(5) Elhenawy, S. E. M.; Khraisheh, M.; AlMomani, F.; Walker, G. Metal-Organic Frameworks as a Platform for CO2 Capture and Chemical Processes: Adsorption, Membrane Separation, Catalytic-Conversion, and Electrochemical Reduction of CO2. *Catalysts* **2020**, *10* (11), 1293.

(6) Li, D. D.; Kassymova, M.; Cai, X. C.; Zang, S. Q.; Jiang, H. L. Photocatalytic CO2 Reduction over Metal-Organic Framework-Based Materials. *Coord. Chem. Rev.* **2020**, *412*, 213262.

(7) Luo, Y. H.; Dong, L. Z.; Liu, J.; Li, S. L.; Lan, Y. Q. From Molecular Metal Complex to Metal-Organic Framework: The CO2 Reduction Photocatalysts with Clear and Tunable Structure. *Coord. Chem. Rev.* **2019**, *390*, 86−126.

(8) Diercks, C. S.; Liu, Y. Z.; Cordova, K. E.; Yaghi, O. M. The Role of Reticular Chemistry in the Design of CO2 Reduction Catalysts. *Nat. Mater.* **2018**, *17* (4), 301−307.

(9) Llabrés i Xamena, F. X.; Corma, A.; Garcia, H. Applications for Metal-Organic Frameworks (MOFs) as Quantum Dot Semiconductors. *J. Phys. Chem. C* **2007**, *111* (1), 80−85.

(10) Alvaro, M.; Carbonell, E.; Ferrer, B.; Llabrés i Xamena, F. X.; Garcia, H. Semiconductor Behavior of a Metal-Organic Framework (MOF). *Chem. Eur. J.* **2007**, *13* (18), 5106−5112.

(11) Zhang, T.; Lin, W. B. Metal-Organic Frameworks for Artificial Photosynthesis and Photocatalysis. *Chem. Soc. Rev.* **2014**, *43* (16), 5982−5993.
(12) Nasalevich, M. A.; Goesten, M. G.; Savenije, T. J.; Kapteijn, F.; Gascon, J. Enhancing Optical Absorption of Metal-Organic Frameworks for Improved Visible Light Photocatalysis. *Chem. Commun.* **2013**, *49* (90), 10575−10577.
(13) Hendon, C. H.; Tiana, D.; Walsh, A. Conductive Metal-Organic Frameworks and Networks: Fact or Fantasy? *Phys. Chem. Chem. Phys.* **2012**, *14* (38), 13120−13132.
(14) Mancuso, J. L.; Mroz, A. M.; Le, K. N.; Hendon, C. H. Electronic Structure Modeling of Metal-Organic Frameworks. *Chem. Rev.* **2020**, *120* (16), 8641−8715.
(15) Liu, J.; Goetjen, T. A.; Wang, Q. I.; Knapp, J. G.; Wasson, M. C.; Yang, Y.; Syed, Z. H.; Delferro, M.; Notestein, J. M.; Farha, O. K.; et al. Mof-Enabled Confinement and Related Effects for Chemical Catalyst Presentation and Utilization. *Chem. Soc. Rev.* **2022**, *51* (3), 1045−1097.
(16) Majewski, M. B.; Peters, A. W.; Wasielewski, M. R.; Hupp, J. T.; Farha, O. K. Metal-Organic Frameworks as Platform Materials for Solar Fuels Catalysis. *ACS. Energy. Lett.* **2018**, *3* (3), 598−611.
(17) Fu, Y.; Sun, D.; Chen, Y.; Huang, R.; Ding, Z.; Fu, X.; Li, Z. An Amine-Functionalized Titanium Metal-Organic Framework Photocatalyst with Visible-Light-Induced Activity for CO2 Reduction. *Angew. Chem., Int. Ed. Engl.* **2012**, *51* (14), 3364−3367.
(18) Bai, Y.; Dou, Y. B.; Xie, L. H.; Rutledge, W.; Li, J. R.; Zhou, H. C. Zr-Based Metal-Organic Frameworks: Design, Synthesis, Structure, and Applications. *Chem. Soc. Rev.* **2016**, *45* (8), 2327−2367.
(19) Howarth, A. J.; Liu, Y. Y.; Li, P.; Li, Z. Y.; Wang, T. C.; Hupp, J.; Farha, O. K. Chemical, Thermal and Mechanical Stabilities of Metal-Organic Frameworks. *Nat. Rev. Mater.* **2016**, *1* (3), 15018.
(20) Sun, D. R.; Fu, Y. H.; Liu, W. J.; Ye, L.; Wang, D. K.; Yang, L.; Fu, X. Z.; Li, Z. H. Studies on Photocatalytic CO2 Reduction over NH2-Uio-66(Zr) and Its Derivatives: Towards a Better Understanding of Photocatalysis on Metal-Organic Frameworks. *Chem. Eur. J.* **2013**, *19* (42), 14279−14285.
(21) Xu, H. Q.; Hu, J. H.; Wang, D. K.; Li, Z. H.; Zhang, Q.; Luo, Y.; Yu, S. H.; Jiang, H. L. Visible-Light Photoreduction of CO2 in a Metal-Organic Framework: Boosting Electron-Hole Separation via Electron Trap States. *J. Am. Chem. Soc.* **2015**, *137* (42), 13440−13443.
(22) Sun, M. Y.; Yan, S. Y.; Sun, Y. J.; Yang, X. H.; Guo, Z. F.; Du, J. F.; Chen, D. S.; Chen, P.; Xing, H. Z. Enhancement of Visible-Light-Driven CO2 Reduction Performance Using an Amine-Functionalized Zirconium Metal-Organic Framework. *Dalton. Trans.* **2018**, *47* (3), 909−915.
(23) Zeng, J. Y.; Wang, X. S.; Xie, B. R.; Li, Q. R.; Zhang, X. Z. Large pi-Conjugated Metal-Organic Frameworks for Infrared-Light-Driven CO2 Reduction. *J. Am. Chem. Soc.* **2022**, *144* (3), 1218−1231.
(24) Qiu, Y. C.; Yuan, S.; Li, X. X.; Du, D. Y.; Wang, C.; Qin, J. S.; Drake, H. F.; Lan, Y. Q.; Jiang, L.; Zhou, H. C. Face-Sharing Archimedean Solids Stacking for the Construction of Mixed-Ligand Metal-Organic Frameworks. *J. Am. Chem. Soc.* **2019**, *141* (35), 13841−13848.
(25) Chen, D. S.; Xing, H. Z.; Wang, C. G.; Su, Z. M. Highly Efficient Visible-Light-Driven CO2 Reduction to Formate by a New Anthracene-Based Zirconium MOF via Dual Catalytic Routes. *J. Mater. Chem. A* **2016**, *4* (7), 2657−2662.
(26) Qin, J. S.; Yuan, S.; Zhang, L.; Li, B.; Du, D. Y.; Huang, N.; Guan, W.; Drake, H. F.; Pang, J. D.; Lan, Y. Q.; et al. Creating Well-Defined Hexabenzocoronene in Zirconium Metal-Organic Framework by Postsynthetic Annulation. *J. Am. Chem. Soc.* **2019**, *141* (5), 2054−2060.
(27) Elcheikh Mahmoud, M.; Audi, H.; Assoud, A.; Ghaddar, T. H.; Hmadeh, M. Metal-Organic Framework Photocatalyst Incorporating Bis(4 ′-(4-carboxyphenyl)-terpyridine)ruthenium(II) for Visible-Light-Driven Carbon Dioxide Reduction. *J. Am. Chem. Soc.* **2019**, *141* (17), 7115−7121.
(28) Wang, C.; Xie, Z. G.; deKrafft, K. E.; Lin, W. L. Doping Metal-Organic Frameworks for Water Oxidation, Carbon Dioxide Reduction, and Organic Photocatalysis. *J. Am. Chem. Soc.* **2011**, *133* (34), 13445−13454.
(29) Hu, X. F.; Chen, P. C.; Zhang, C. K.; Wang, Z. Y.; Wang, C. Energy Transfer on a Two-Dimensional Antenna Enhances the Photocatalytic Activity of CO2 Reduction by Metal-Organic Layers. *Chem. Commun.* **2019**, *55* (65), 9657−9660.
(30) Zhang, H. B.; Wei, J.; Dong, J. C.; Liu, G. G.; Shi, L.; An, P. F.; Zhao, G. X.; Kong, J. T.; Wang, X. J.; Meng, X. G.; et al. Efficient Visible-Light-Driven Carbon Dioxide Reduction by a Single-Atom Implanted Metal-Organic Framework. *Angew. Chem., Int. Ed.* **2016**, *55* (46), 14310−14314.
(31) Fei, H. H.; Sampson, M. D.; Lee, Y.; Kubiak, C. P.; Cohen, S. M. Photocatalytic CO2 Reduction to Formate Using a Mn(I) Molecular Catalyst in a Robust Metal-Organic Framework. *Inorg. Chem.* **2015**, *54* (14), 6821−6828.
(32) Karmakar, S.; Barman, S.; Rahimi, F. A.; Maji, T. K. Covalent Grafting of Molecular Photosensitizer and Catalyst on MOF-808: Effect of Pore Confinement Toward Visible Light-Driven CO2 Reduction in Water. *Energy Environ. Sci.* **2021**, *14* (4), 2429−2440.
(33) Li, J.; Huang, H. L.; Xue, W. J.; Sun, K.; Song, X. H.; Wu, C. R.; Nie, L.; Li, Y.; Liu, C. Y.; Pan, Y.; et al. Self-Adaptive Dual-Metal-Site Pairs in Metal-Organic Frameworks for Selective CO2 Photoreduction to CH4. *Nat. Catal.* **2021**, *4* (8), 719−729.
(34) Hao, Y. C.; Chen, L. W.; Li, J. N.; Guo, Y.; Su, X.; Shu, M.; Zhang, Q. H.; Gao, W. Y.; Li, S. W.; Yu, Z. L.; et al. Metal-Organic Framework Membranes With Single-Atomic Centers for Photocatalytic CO2 and O2 Reduction. *Nat. Commun.* **2021**, *12* (1), 12.
(35) Wang, G.; He, C. T.; Huang, R.; Mao, J. J.; Wang, D. S.; Li, Y. D. Photoinduction of Cu Single Atoms Decorated on UiO-66-NH2 for Enhanced Photocatalytic Reduction of CO2 to Liquid Fuels. *J. Am. Chem. Soc.* **2020**, *142* (45), 19339−19345.
(36) Guo, S.; Kong, L. H.; Wang, P.; Yao, S.; Lu, T. B.; Zhang, Z. M. Switching Excited State Distribution of Metal-Organic Framework for Dramatically Boosting Photocatalysis. *Angew. Chem., Int. Ed.* **2022**, *61* (30), e202206193.
(37) Chen, Y. J.; Li, P.; Zhou, J. W.; Buru, C. T.; Dordevic, L.; Li, P. H.; Zhang, X.; Cetin, M. M.; Stoddart, J. F.; Stupp, S. I.; et al. Integration of Enzymes and Photosensitizers in a Hierarchical Mesoporous Metal-Organic Framework for Light-Driven CO2 Reduction. *J. Am. Chem. Soc.* **2020**, *142* (4), 1768−1773.
(38) Chen, D. S.; Guo, Z. F.; Li, B.; Xing, H. Z. Visible-Light-Driven Photocatalytic CO2 Reduction to Formate Over a Zirconium-Porphyrin Metal-Organic Framework with shp-a Topology. *New. J. Chem.* **2022**, *46* (34), 16297−16302.
(39) de Miguel, M.; Ragon, F.; Devic, T.; Serre, C.; Horcajada, P.; Garcia, H. Evidence of Photoinduced Charge Separation in the Metal-Organic Framework MIL-125(Ti)-NH2. *ChemPhysChem* **2012**, *13* (16), 3651−3654.
(40) Nasalevich, M. A.; Hendon, C. H.; Santaclara, J. G.; Svane, K.; van der Linden, B.; Veber, S. L.; Fedin, M. V.; Houtepen, A. J.; van der Veen, M. A.; Walsh, A. Electronic Origins of Photocatalytic Activity in d(0) Metal Organic Frameworks. *Sci. Rep.* **2016**, *6*, 23676.
(41) Horiuchi, Y.; Toyao, T.; Saito, M.; Mochizuki, K.; Iwata, M.; Higashimura, H.; Anpo, M.; Matsuoka, M. Visible-Light-Promoted Photocatalytic Hydrogen Production by Using an Amino-Functionalized Ti(IV) Metal-Organic Framework. *J. Phys. Chem. C* **2012**, *116* (39), 20848−20853.
(42) Wu, X. P.; Gagliardi, L.; Truhlar, D. G. Cerium Metal-Organic Framework for Photocatalysis. *J. Am. Chem. Soc.* **2018**, *140* (25), 7904−7912.
(43) Li, X. L.; Yu, J. R.; Gosztola, D. J.; Fry, H. C.; Deria, P. Wavelength-Dependent Energy and Charge Transfer in MOF: A Step toward Artificial Porous Light-Harvesting System. *J. Am. Chem. Soc.* **2019**, *141* (42), 16849−16857.
(44) Benseghir, Y.; Sole-Daura, A.; Cairnie, D. R.; Robinson, A. L.; Duguet, M.; Mialane, P.; Gairola, P.; Gomez-Mingot, M.; Fontecave, M.; Iovan, D.; et al. Unveiling the Mechanism of the Photocatalytic

https://doi.org/10.1021/acs.jpclett.3c00049
J. Phys. Chem. Lett. 2023, 14, 4334−4341

Reduction of CO2 to Formate Promoted by Porphyrinic Zr-Based Metal-Organic Frameworks. *J. Mater. Chem. A* **2022**, *10* (35), 18103−18115.
(45) Schneider, J.; Bahnemann, D. W. Undesired Role of Sacrificial Reagents in Photocatalysis. *J. Phys. Chem. Lett.* **2013**, *4* (20), 3479−3483.
(46) Cannon, G. C.; Heinhorst, S.; Kerfeld, C. A. Carboxysomal Carbonic Anhydrases: Structure and Role in Microbial CO2 Fixation. *Biochim. Biophys. Acta* **2010**, *1804* (2), 382−392.
(47) Bien, C. E.; Chen, K. K.; Chien, S. C.; Reiner, B. R.; Lin, L. C.; Wade, C. R.; Ho, W. S. W. Bioinspired Metal-Organic Framework for Trace CO2 Capture. *J. Am, Chem. Soc.* **2018**, *140* (40), 12662−12666.
(48) Alezi, D.; Spanopoulos, I.; Tsangarakis, C.; Shkurenko, A.; Adil, K.; Belmabkhout, Y.; O'Keeffe, M.; Eddaoudi, M.; Trikalitis, P. N. Reticular Chemistry at Its Best: Directed Assembly of Hexagonal Building Units into the Awaited Metal-Organic Framework with the Intricate Polybenzene Topology, pbz-MOF. *J. Am. Chem. Soc.* **2016**, *138* (39), 12767−12770.
(49) Yan, X.; Wang, K.; Xu, X.; Wang, S.; Ning, Q.; Xiao, W.; Zhang, N.; Chen, Z.; Chen, C. Bronsted Basicity in Metal-Organic Framework-808 and Its Application in Base-Free Catalysis. *Inorg. Chem.* **2018**, *57* (14), 8033−8036.
(50) Korhonen, S. T.; Calatayud, M.; Krause, A. O. I. Structure and Stability of Formates and Carbonates on Monoclinic Zirconia: A Combined Study by Density Functional Theory and Infrared Spectroscopy. *J. Phys. Chem. C* **2008**, *112* (41), 16096−16102.
(51) Dobson, K. D.; McQuillan, A. J. An Infrared Spectroscopic Study of Carbonate Adsorption to Zirconium Dioxide Sol-Gel Films From Aqueous Solutions. *Langmuir* **1997**, *13* (13), 3392−3396.
(52) Bachiller-Baeza, B.; Rodriguez-Ramos, I.; Guerrero-Ruiz, A. Interaction of Carbon Dioxide With the Surface of Zirconia Polymorphs. *Langmuir* **1998**, *14* (13), 3556−3564.
(53) Bianchi, D.; Chafik, T.; Khalfallah, M.; Teichner, S. J. Intermediate Species on Zirconia Supported Methanol Aerogel Catalysts 0.4. Adsorption of Carbon-Dioxide. *Appl. Catal. a-Gen.* **1994**, *112* (2), 219−235.
(54) Garand, E.; Wende, T.; Goebbert, D. J.; Bergmann, R.; Meijer, G.; Neumark, D. M.; Asmis, K. R. Infrared Spectroscopy of Hydrated Bicarbonate Anion Clusters: HCO3-(H2O)(1−10). *J. Am. Chem. Soc.* **2010**, *132* (2), 849−856.
(55) Yan, X. D.; Wang, K.; Xu, X. C.; Wang, S. H.; Ning, Q.; Xiao, W. M.; Zhang, N.; Chen, Z. J.; Chen, C. Bronsted Basicity in Metal-Organic Framework-808 and Its Application in Base-Free Catalysis. *Inorg. Chem.* **2018**, *57* (14), 8033−8036.
(56) Veyland, A.; Rimbault, J.; Dupont, L.; Pierrard, J. C.; Aplincourt, M.; Bourg, S.; Nuzillard, J. M.; Angiboust, J. F. Coordination Mode and Kinetic Behavior of the Tetracarbonatozirconate Ion. *Helv. Chim. Acta* **1999**, *82* (11), 2003−2014.
(57) Takasaki, F.; Fujiwara, K.; Nakajima, Y.; Nishikawa, T.; Masu, H.; Imanari, M.; Hidaka, Y.; Ogawa, N. A Monomeric [Zr(CO3)(4)](4-) Complex in an Ammonium Zirconium Carbonate Aqueous Solution Studied by Extended X-Ray Absorption Fine Structure, Raman and Nuclear Magnetic Resonance Spectroscopy. *Dalton Trans* **2015**, *44* (2), 645−652.
(58) Chu, J.; Ke, F. S.; Wang, Y. X.; Feng, X. M.; Chen, W. H.; Ai, X. P.; Yang, H. X.; Cao, Y. L. Facile and Reversible Digestion and Regeneration of Zirconium-Based Metal-Organic Frameworks. *Commun. Chem.* **2020**, *3* (1), 5.
(59) Thomson, S. A. J.; Niklas, J.; Mardis, K. L.; Mallares, C.; Samuel, I. D. W.; Poluektov, O. G. Charge Separation and Triplet Exciton Formation Pathways in Small-Molecule Solar Cells as Studied by Time-Resolved EPR Spectroscopy. *J. Phys. Chem. C* **2017**, *121* (41), 22707−22719.
(60) Hintze, C.; Steiner, U. E.; Drescher, M. Photoexcited Triplet State Kinetics Studied by Electron Paramagnetic Resonance Spectroscopy. *ChemPhysChem* **2017**, *18* (1), 6−16.
(61) Budil, D. E.; Thurnauer, M. C. The Chlorophyll Triplet-State as a Probe of Structure and Function in Photosynthesis. *Biochim. Biophys. Acta* **1991**, *1057* (1), 1−41.
(62) Tait, C. E.; Neuhaus, P.; Peeks, M. D.; Anderson, H. L.; Timmel, C. R. Transient EPR Reveals Triplet State Delocalization in a Series of Cyclic and Linear pi-Conjugated Porphyrin Oligomers. *J. Am. Chem. Soc.* **2015**, *137* (25), 8284−8293.
(63) Redman, A. J.; Moise, G.; Richert, S.; Peterson, E. J.; Myers, W. K.; Therien, M. J.; Timmel, C. R. EPR of Photoexcited Triplet-State Acceptor Porphyrins. *J. Phys. Chem. C* **2021**, *125* (21), 11782−11790.
(64) Wu, Y. L.; Young, R. M.; Frasconi, M.; Schneebeli, S. T.; Spenst, P.; Gardner, D. M.; Brown, K. E.; Wurthner, F.; Stoddart, J. F.; Wasielewski, M. R. Ultrafast Photoinduced Symmetry-Breaking Charge Separation and Electron Sharing in Perylenediimide Molecular Triangles. *J. Am. Chem. Soc.* **2015**, *137* (41), 13236−13239.
(65) Wu, H.; Wang, Y.; Song, B.; Wang, H. J.; Zhou, J. W.; Sun, Y. X.; Jones, L. O.; Liu, W. Q.; Zhang, L.; Zhang, X. A Contorted Nanographene Shelter. *Nat. Commun.* **2021**, *12* (1), 5191.
(66) Moshniaha, L.; Zyla-Karwowska, M.; Chmielewski, P. J.; Lis, T.; Cybinska, J.; Gonka, E.; Oschwald, J.; Drewello, T.; Rivero, S. M.; Casado, J.; et al. Aromatic Nanosandwich Obtained by sigma-Dimerization of a Nanographenoid pi-Radical. *J. Am. Chem. Soc.* **2020**, *142* (7), 3626−3635.
(67) Chen, X. Y.; Wang, X. Y.; Zhou, Z. Y.; Li, Y. Z.; Sui, Y. X.; Ma, J.; Wang, X. P.; Power, P. P. Reversible sigma-Dimerizations of Persistent Organic Radical Cations. *Angew. Chem., Int. Ed.* **2013**, *52* (2), 589−592.
(68) Kumagai, T.; Shiotari, A.; Okuyama, H.; Hatta, S.; Aruga, T.; Hamada, I.; Frederiksen, T.; Ueba, H. H-Atom Relay Reactions in Real Space. *Nat. Mater.* **2012**, *11* (2), 167−172.
(69) Wodrich, M. D.; Hu, X. L. Natural Inspirations for Metal-Ligand Cooperative Catalysis. *Nat. Rev. Chem.* **2018**, *2* (1), 0099.
(70) Sullivan, I.; Goryachev, A.; Digdaya, I. A.; Li, X. Q.; Atwater, H. A.; Vermaas, D. A.; Xiang, C. X. Coupling Electrochemical CO2 Conversion with CO2 Capture. *Nat. Catal.* **2021**, *4* (11), 952−958.
(71) Yamazaki, Y.; Miyaji, M.; Ishitani, O. Utilization of Low-Concentration CO2 with Molecular Catalysts Assisted by CO2-Capturing Ability of Catalysts, Additives, or Reaction Media. *J. Am. Chem. Soc.* **2022**, *144* (15), 6640−6660.
(72) Siegel, R. E.; Pattanayak, S.; Berben, L. A. Reactive Capture of CO2: Opportunities and Challenges. *ACS Catal.* **2023**, *13* (1), 766−784.
(73) Frank, S. N.; Bard, A. J. Semiconductor Electrodes 0.12. Photoassisted Oxidations and Photoelectrosynthesis at Polycrystalline Tio2 Electrodes. *J. Am. Chem. Soc.* **1977**, *99* (14), 4667−4675.
(74) Fujishima, A.; Kato, T.; Maekawa, E.; Honda, K. Mechanism of the Current Doubling Effect 0.1. The Zno Photoanode in Aqueous-Solution of Sodium Formate. *B. Chem. Soc. Jpn.* **1981**, *54* (6), 1671−1674.
(75) Gould, I. R.; Lenhard, J. R.; Muenter, A. A.; Godleski, S. A.; Farid, S. Two-Electron Sensitization: A New Concept for Silver Halide Photography. *J. Am. Chem. Soc.* **2000**, *122* (48), 11934−11943.

https://doi.org/10.1021/acs.jpclett.3c00049
J. Phys. Chem. Lett. 2023, 14, 4334−4341